Title

Driving useful morphological changes in magnetic nanoparticle structures through the application of acoustic waves and magnetic fields

Journal

Applied Physics Letters, 113(3)

ISSN

0003-6951

Authors

Huang, An
Miansari, Morteza
Friend, James

Publication Date

2018-07-16

DOI

10.1063/1.5037086

Peer reviewed

Driving useful morphological changes in magnetic nanoparticle structures through the application of acoustic waves and magnetic fields

An Huang, Morteza Miansari, and James Friend

Citation: Appl. Phys. Lett. **113**, 034103 (2018); doi: 10.1063/1.5037086
View online: https://doi.org/10.1063/1.5037086
View Table of Contents: http://aip.scitation.org/toc/apl/113/3
Published by the American Institute of Physics

Driving useful morphological changes in magnetic nanoparticle structures through the application of acoustic waves and magnetic fields

An Huang,[1] Morteza Miansari,[2,a)] and James Friend[3]
[1]Department of Materials Science and Engineering, University of California, San Diego, 9500 Gilman Drive, SME Building, Room 320, La Jolla, California 92903, USA
[2]Department of Mechanical and Aerospace Engineering, University of California, San Diego, California 92093, USA
[3]Departments of Mechanical and Aerospace Engineering and Materials Science and Engineering, University of California, San Diego, 9500 Gilman Drive, SME Building, Room 345F, La Jolla, California 92903, USA

(Received 20 April 2018; accepted 28 June 2018; published online 20 July 2018)

The growing interest in acoustic manipulation of particles in micro to nanofluidics using surface acoustic waves, together with the many applications of magnetic nanoparticles—whether individual or in arrays—underpins our discovery of how these forces can be used to rapidly, easily, and irreversibly form 1D chains and 2D films. These films and chains are difficult to produce by other methods yet offer many advantages over suspensions of individual nanoparticles by making use of the scale of the structures formed, 10^{-9} to 10^{-5} m, and by taking a balance of the relevant external and interparticle forces, the underlying mechanisms responsible for the phenomena become apparent. For loosely connected 1D chains, the magnetic field alone is sufficient, though applying an acoustic field drives a topology change to interconnected loops of ~10–100 particles. Increasing the acoustic field intensity drives a transition from these looped structures to dense 2D arrays via interparticle Bjerknes forces. Inter-particle drainage of the surrounding fluid leaves these structures intact after removal of the externally applied forces. The self-evident morphology transitions depend solely upon the relative amplitudes of the Brownian, Bjerknes, and magnetic forces. *Published by AIP Publishing.* https://doi.org/10.1063/1.5037086

Self-assembly is touted as a useful bottom-up alternative to traditional top-down fabrication techniques, improving material performance and utility of nanomaterials via superior collective physical and chemical properties in transitioning from zero to one (1D) or two dimensionally (2D) ordered patterns.[1] Such patterns, self-assembled on a liquid interface, may prove useful in emerging applications.[2] For example, 1D chains facilitate single electron transport,[3] waveguiding,[4] and energy transfer[5] along the chain axis. Likewise, 2D nanoparticle (NP) films have been considered for biosensors,[6] targeted drug delivery,[7] photonic crystals,[8] and high-density data storage.[9]

Here, we used magnetite (Fe_3O_4) as our precursor NP due to its promising intrinsic properties, natural abundance, non-toxicity, chemical stability, biocompatibility, and ferrimagnetism. It is a ferrite with a cubic structure (Fd3m), exhibiting unique electric and magnetic properties due to electron transfer between Fe^{2+} and Fe^{3+} at the octahedral sites, and has long been considered a useful NP.[10–12]

Due to the useful properties of Fe_3O_4 NP agglomerates, a variety of techniques have been developed to produce 1D chains and 2D films, including alumina templating,[13] electrodeposition,[14] and the imposition of external magnetic fields from 0.2 to 0.6 T[15] for 1D structures and Langmuir-Blodgett films,[16] spin coating,[16] electrophoretic deposition,[17] laser interference lithography, and emulsion[18] for 2D structures. Inevitably, weak and defect-laden structures are formed from these methods unless external forces or chemical binders are introduced which unfortunately reduce the utility of the NP chains and films.[19,20] Moreover, the complexity and cost of these methods relegate them to a relatively small market niche.[13,21]

We present a fast, cost-effective, and additive-free approach to obtain 1D chains and 2D films composed of Fe_3O_4 NPs in the presence of 0.2–0.4 T external magnetic fields and Rayleigh surface acoustic wave (SAW)-driven acoustic waves, and consider the mechanisms responsible for the self-assembly via a combination of scaling and experimental results from a simple prototype.

The experimental setup is depicted in Fig. 1. A sinusoidal electric signal generated by a function generator (SG 380, Stanford Research Systems, Sunnyvale, CA) and a high frequency amplifier (ZHL-1-2W, Mini-Circuits, Brooklyn, NY, USA) was used to drive a 127.86° *Y*-rotated *X*-propagating cut of lithium niobate [$LiNbO_3$ (LN), 500 μm thick, Roditi, London, UK] surface acoustic wave device via a simple unweighted Al/Cr interdigital transducer[22] of 28 finger pairs deposited using lift-off lithography[23] with gap and finger widths of 10 μm ($\lambda_{SAW}/4$), producing a resonant frequency of $f_s = c_s/\lambda_{SAW} = 100$ MHz. A 3 $\mu\ell$ deionized (DI) water sessile drop with a 0.1 $\mu\ell$ Fe_3O_4 NP in toluene (5 mg/ml) was placed on LN (Sigma Aldrich, St. Louis, MO, USA). The particles were strongly bound to the free interface of the droplet by surface tension.[24] The SAW passes acoustic energy into the drop at the Rayleigh angle, $\sin^{-1}\theta = c_l/c_s = 22°$, where $c_l = 1485$ m/s is the speed of sound in water, producing acoustic streaming in the sessile drop.[25] A reasonable estimate for the maximum particle velocity in a media continuously supporting an acoustic wave without failure is ~1 m/s and independent of

a)Present address: Department of Radiology, School of Medicine, Stanford University, 291 Campus Drive, Stanford, California 94305, USA.

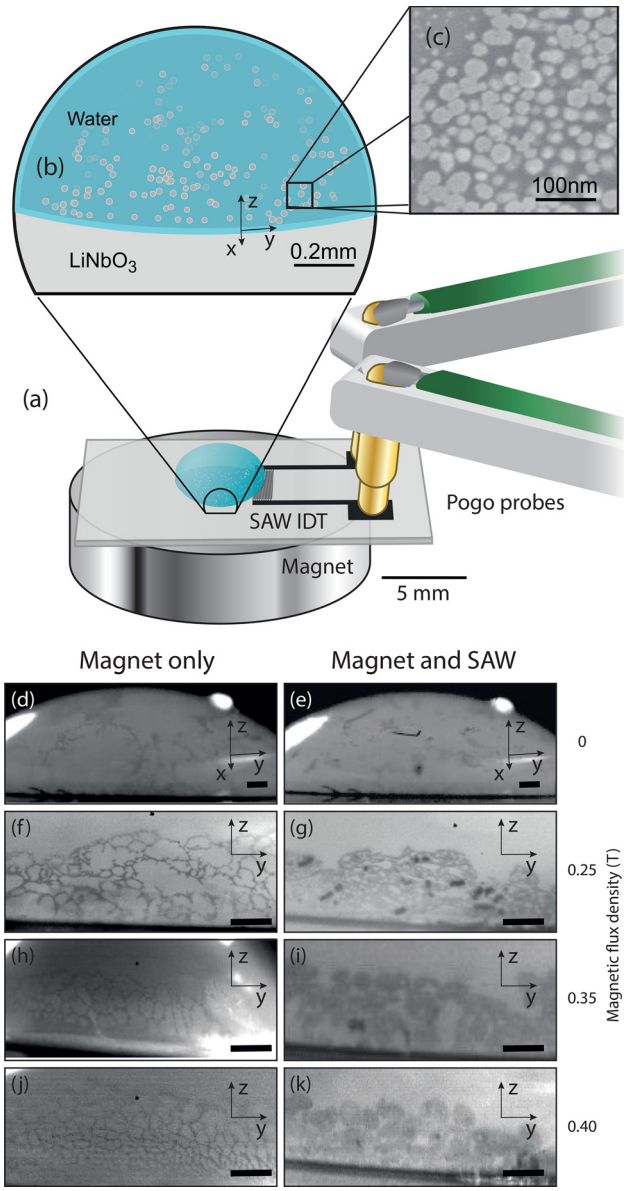

FIG. 1. (a) A 3 $\mu\ell$ DI water sessile droplet with 0.1 $\mu\ell$ Fe_3O_4 NP produced via solvent exchange from toluene is placed upon a bare LN surface (size ~1 mm) incorporating a 100 MHz SAW device (wavelength 40 μm). The ~10 nm Fe_3O_4 NP (c) resides upon the fluid-air interface. With only the application of (d) 0, (f) 0.25, (h) 0.35, and (j) 0.4 T external magnetic field fluxes, respectively, 1D chains are produced; (e), (g), (i), and (k) SAW are necessary to produce 2D films. Here, 10 s of SAW was applied to obtain the images [(d)–(k): scale bar is 500 μm].

the resonant frequency.[26] At 100 MHz, the SAW displacement amplitude is extremely small at $\mathcal{O}(1\,\text{nm})$ but produces an extremely high surface acceleration of $\mathcal{O}(10^8\text{m/s}^2)$. Despite this, in our experiments in this study, the shape of the drop did not change nor oscillate, due to the low power SAW used here.

The morphologies and radii of the Fe_3O_4 NPs were determined by environmental scanning electron microscopy [ESEM, Philips XL 30, FEI, Hillsboro, Oregon, at 10 keV; see Fig. 1(c)]: the average radius of the particles is 10 nm with a standard error of 0.4% ($n = 150$). External magnetic fields of 200–400 mT were produced using magnets (Grade N42, K&J Magnet, Pipersville, PA, USA) of the same 9.525 mm diameter but different thicknesses. The motion of the Fe_3O_4 NPs was recorded with a high-speed camera (FASTCAM Mini UX100, Photron, Tokyo, Japan) and microscope (K2/CF-4, Infinity, Boulder, CO, USA). The images were analyzed using MATLAB (Mathworks, Natick, MA USA) and ImageJ (National Institutes of Health, Bethesda, MD USA). The phase map, Fig. 2, illustrates how the applied SAW power and magnetic field leads to 1D chain assembly and 2D film formation of the Fe_3O_4 NP on a 3 $\mu\ell$ sessile drop. As expected, chains of NP assemble (region I) without SAW and with or without an external magnetic force.[15,27] The Brownian force is known to dominate and produce random floating chains in the absence of SAW and magnetic fields from dispersed suspensions of magnetic NPs.[27]

Upon introducing a magnetic field, the Fe_3O_4 NPs orient along the magnetic field lines[27] in head-to-tail, dipolar aligned chains to minimize the overall dipolar potential energy.[28–30] These chains appear around the periphery of the drop and near the contact line, with a significantly reduced concentration of particles at the top of the drop. Interestingly, a dense honeycomb-like structure is formed upon application of a stronger magnetic field, believed to be due to the increase in the induced inter-particle magnetic forces.[30,31] The as-prepared NP states under 0.25, 0.35, and 0.4 T external magnetic field fluxes are shown in Figs. 1(f), 1(h), and 1(j), respectively. The average Einstein-Stokes' hydrodynamic radius (r_h) of the chains is around 3 μm [Fig. 3(b)] using $r_h = (\frac{3\eta M}{10\pi N})^{1/3}$, where η is the intrinsic viscosity, M is the molecular weight (233 g/mol for Fe_3O_4), and N is Avogadro's number.[32] By computing the Minkowski–Bouligand (MB)

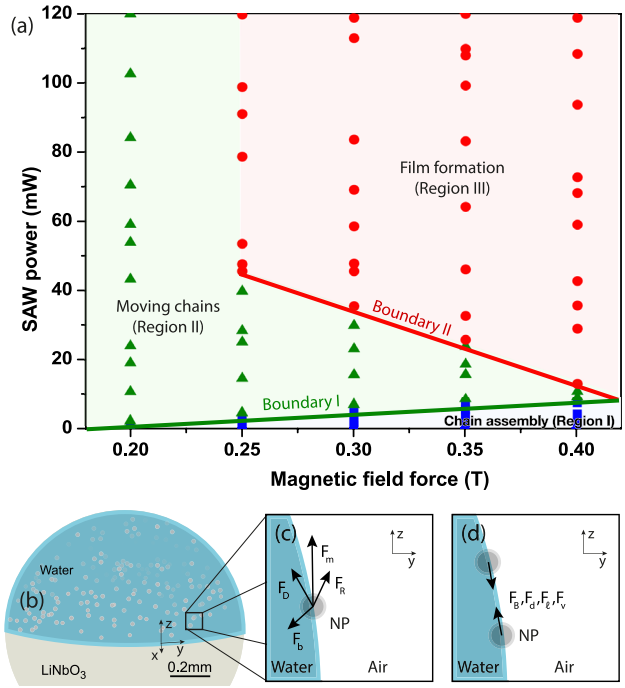

FIG. 2. (a) Phase diagram depicting chain assembly (I), chain movement (II), and film formation (III) regions as a function of SAW power (0–120 mW) and magnetic field strength (0.2–0.4 T). Above 120 mW, the 3 $\mu\ell$ DI water droplet translates across the LN surface, so 120 mW is the upper limit in applied power for our experiments. (b) The directions of the forces experienced by the Fe_3O_4 NP present around the periphery of the drop, including the external magnetic (F_m), dipolar (F_d), Brownian (F_b), van der Waals (F_v), lateral capillary (F_l), SAW radiation (F_R), drag (F_D), and Bjerknes (F_B) forces.

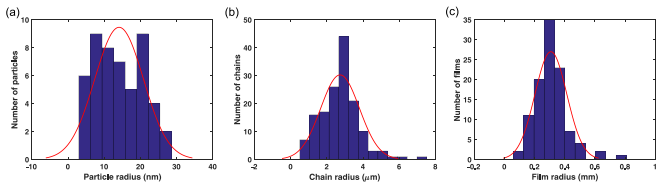

FIG. 3. Histogram (blue bar) with Gaussian distribution (red line) plots of the (a) 0D particles, (b) 1D chains and, (c) 2D film size distributions.

dimension, d_{MB}, via box counting[33] from the NP images in Fig. 1, we find (see Fig. SI1) that the dimension of the NP morphology remains nearly 1D with even a strong 0.4 T magnetic field: $d_{MB} \approx 1.21$. Upon applying a combination of a 0.25 T or 0.4 T magnetic field and SAW, the NP morphology becomes nearly two-dimensional, with $d_{MB} \approx 1.79$ or 1.92, respectively.

Boundary I ($B \propto P_{SAW}$) is reached while increasing the SAW power P_{SAW} from zero [Fig. 2(a)], where B is the magnetic field strength. The boundary indicates the minimum power required to produce chain motion due to SAW-driven acoustic streaming, increasing linearly, albeit weakly with magnetic field flux, indicating that the acoustic power required to overcome the magnetic dipole-driven stability of the interlinked chains to transport them upon the free fluid interface grows with an increasing magnetic field. Figure 1(g) is representative of the NP morphology in this region: the interstitial spacing between the chains is reduced after 10 s of SAW streaming at 115 mW power while a 0.25 T magnetic field is being applied. However, a 2D film does not form.

Boundary II ($B^{-1} \propto P_{SAW}$) indicates the transition to sufficient SAW power and magnetic force to form 2D NP films. For NP chains formed under larger magnetic forces, less SAW power is needed to form the 2D Fe_3O_4 NP film. The interchain spacing is known to be reduced with stronger external magnetic forces[30,31] and thus it is reasonable to expect this outcome. However, below 0.25 T, there is no film formation at any SAW power. The scattering of acoustic waves from the NPs and structures formed from those NPs exerts a Bjerknes force between them, the magnitude and sign of which depends upon the spacing and particle size as indicated in Fig. 4(b). When the interchain spacing is larger than 400 μm, the induced Bjerknes forces between the NP structures are generally constant and repulsive, separating the Fe_3O_4 NPs. When the spacing is less than 400 μm, the Bjerknes forces depend upon the spacing, but grow more negative as the spacing of the NP structures is reduced. This predicts the observed experimental results [Fig. 1(e)], where the average Fe_3O_4 interchain spacing is consistently $\sim$400 μm when the external magnetic force is below 0.25 T.

Crossing boundary II, region III is reached, where 2D films are formed with both SAW and magnetic fields [Fig. 2(a)]. Figures 1(i) and 1(k) provide example 2D films formed in this region from 10 s of 115 mW SAW with 0.25 and 0.4 T magnetic fields, respectively. The effective hydrodynamic radii of these 2D films, $\sim$3 mm, are provided in Fig. 3(c). These 2D films remain intact until the water evaporates, and often remain even until dried.

Beyond 120 mW SAW power, we see droplet translation from SAW-driven acoustic streaming within and acoustic

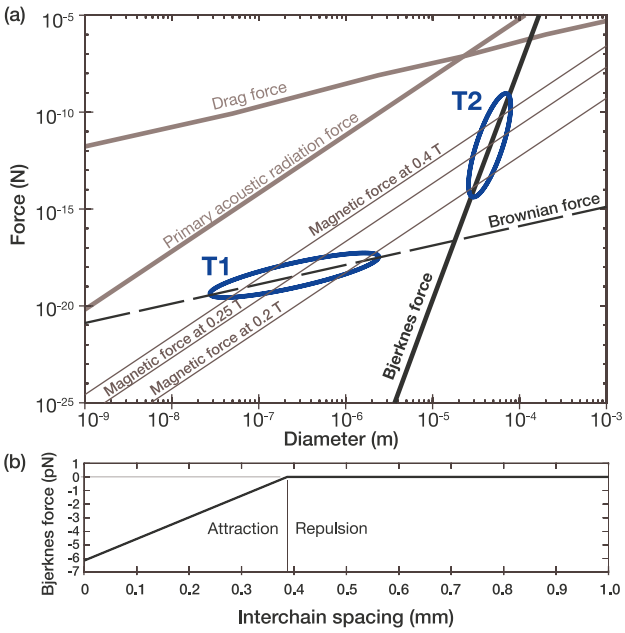

FIG. 4. (a) Dominant forces on the Fe_3O_4 NP particles floating on the liquid surface in magnetic and acoustic fields as a function of particle radii. (b) Relationship between interchain spacing and the Bjerknes force. The critical point is 400 μm, where the Bjerknes force transits from negative to positive values (though nearly zero).

pressure on the free fluid interface that together overwhelm the drop's contact line tension.[34]

To understand the chain assembly and film formation upon application of magnetic fields and SAW, we further examine the forces involved as a function of the hydrodynamic radii of the NP and chains and films formed from them. According to Newton's second law, the balances of forces on an object moving on the free fluid interface while exposed to a magnetic and acoustic field are shown in Eq. (1) and illustrated in Fig. 2(b)

$$m_p \frac{d\mathbf{v}_p}{dt} = F_m\mathbf{e}_m + F_d\mathbf{e}_d + F_b\mathbf{e}_b + F_v\mathbf{e}_v + F_l\mathbf{e}_l + F_R\mathbf{e}_R + F_D\mathbf{e}_D + F_B\mathbf{e}_B, \quad (1)$$

where m_p is the object mass and $d\mathbf{v}_p/dt$ its acceleration; the external magnetic F_m,[35] dipolar F_d,[36] Brownian F_b,[37] van der Waals F_v,[38] lateral capillary F_l,[39] primary SAW radiation F_R,[40] drag F_D,[41] and the Bjerknes F_B[42] forces may be present. The unit vectors $\mathbf{e}_m$, $\mathbf{e}_d$, $\mathbf{e}_b$, $\mathbf{e}_v$, $\mathbf{e}_l$, $\mathbf{e}_R$, $\mathbf{e}_D$, and $\mathbf{e}_B$ indicate the forces' direction as grouped into two categories in Fig. 2(b): forces present *between* the objects (F_B, F_d, F_l, and F_v) and external forces present on *all* the objects (F_D, F_m, F_b, and F_R). The forces in the latter category may be ignored: they affect all nearby objects in a similar fashion and therefore are unlikely to lead to a morphology change, *except* for the Brownian force F_b: this force is random and therefore unique to each object.

By contrast, the interparticle forces are crucially important to the NP agglomerate's morphology, and, for any two Fe_3O_4 NPs include the dipolar force, Brownian force, van der Waals force, and the lateral capillary force.[43] The dipolar force is expressed as $F_d = \frac{6\mu_0 V_p m_p^2}{4\pi r^4}$, where $\mu_0 = 7 \times 10^{-20}$ J is the magnetization of the Fe_3O_4 NP and $r = 10$ nm is the radius of each Fe_3O_4 NP.[36] The Brownian force is

$F_b = \sqrt{\frac{6\pi k_B}{\Delta t} T(2r)}$, where $K_B = 1.38 \times 10^{-23}$ J/K is the Boltzmann constant and T is temperature.[37] The Van der Waals force is $F_v = \frac{Ar}{12L^2}$, where $A \sim 35 \times 10^{-12}$ erg is Hamaker's constant for Fe_3O_4 in water[44] and $L = 10$ nm is the distance between two Fe_3O_4 NPs.[38,45] Finally, an attractive capillary force exists between any two Fe_3O_4 NPs on the H_2O surface, expressed as $F_l = 2\pi\gamma \frac{Q_1 Q_2}{L}$, where γ is the surface tension of water and $Q_n \simeq r_n \sin\varphi_n$ is the "capillary charge," characterizing the local deviation of the meniscus shape at the three-phase contact line due to the NP's presence, where r_n and φ_n are the radius of the contact line and the slope at the contact line with respect to the particle's surface, respectively.[46,47]

When the Fe_3O_4 NPs are placed in an external magnetic field, the NPs and their magnetic moments rotate into the direction of the field and increase the magnetic flux density. The magnetic force on each NP is expressed as $F_m = \frac{V_p \Delta\chi}{\mu_o} B(\nabla B)$, where V_p is the volume of the particles, $\Delta\chi = 10^{-5}$ is the susceptibility of Fe_3O_4 relative to the medium (water), $\mu_o = 10^{-6}$ N/A^2 is the permeability of vacuum, and B is the magnetic flux density.[35,48]

Finally, the forces from the fluid upon the NP with SAW include direct acoustic radiation, Stokes drag, and Bjerknes' forces. The direct acoustic radiation force imposed by a traveling wave on an compressible particle—which the NPs are expected to be—was derived by Nadal[40] and is expressed as: $F_R = \frac{2}{3}\pi\rho_w(\xi_0 C_w)^2 (k_0 r)^3 \left(\frac{\beta-1}{\beta}\right) \frac{\epsilon}{\sqrt{2}}$, where ρ_w is the density of water, ξ_0 is the displacement of the incident wave, C_w is the speed of the sound in the water, k_o is the wavenumber, $\beta = \rho_w/\rho_c$, where ρ_c is the Fe_3O_4 density, and $\epsilon = \left(\frac{r^2 w}{v}\right)^{1/2}$ describes the dimensionless relationship among the particle radius (r), frequency (w), and kinematic viscosity (v). Moreover, the Stokes drag upon the particle is $F_D = 6\pi\mu r v$, where μ is the viscosity of H_2O and v is the velocity difference between the surrounding fluid and the NP. Finally, Bjerknes' force, an interparticle force arising from the scattering of the incident acoustic wave, is defined as $F_B = 4\pi r^6 \left[\frac{(\rho_c-\rho_w)^2(3\cos^2\theta-1)}{6\rho_w r^4} V^2(X) - \frac{\omega^2 \rho_w (\beta_c-\beta_w)^2}{9L^2} P^2(X)\right]$,[42] where $V(X)$ is the particle velocity amplitude, β_c is the compressibility of Fe_3O_4 NP, β_w is the compressibility of water, and $P(X)$ is the acoustic pressure amplitude, respectively. Bjerknes' force changes in amplitude *and* from attraction to repulsion as the interparticle chain spacing increases, as shown in Fig. 4(b).

The primary acoustic radiation force and viscous drag force dominate for objects of radii 1 nm to 0.1 mm as shown in Fig. 4(b). However, both of these forces are equally present upon all the objects in the system, and consequently are irrelevant for the NP morphology. Among the remaining forces, the Brownian force dominates objects less than 100 nm in size, the magnetic field flux-derived force dominates those sized between 100 nm and 10^{-4} m, and Bjerknes' force dominates those particles larger than 100 μm in size. Consequently, a single Fe_3O_4 NP (as the average radii of Fe_3O_4 is around 10 nm) forms loosely bound 1D chains, as shown in Fig. 1(d) and seen in past work.[49] Brownian forces dominate the particles at these small scales irrespective of the presence of magnetic or acoustic fields.

When particles randomly agglomerate from Brownian motion to form 1D chains surpassing a hydrodynamic radius of 100 nm, application of a magnetic field causes the attractive magnetic interparticle forces to dominate the chains' behavior. Nanoparticle 1D chains of 100 nm to 10 μm size [Fig. 3(b)] form honeycomb-like structures that only appear upon the application of an external magnetic field. The NPs' dipoles reorient along the field, induce local magnetic fields between neighboring Fe_3O_4 NP, and drive head-to-tail, interparticle attraction that links the chains together for as long as the magnetic field is present.[15,31,50] The transition from Brownian motion to magnetic field-dominated behavior is denoted as the first transition point (T1) between these influences in Fig. 4(a).

As these chains of NPs grow in size from 100 nm to 100 μm in size and 1D to 2D in dimensionality, the secondary acoustic force present between the objects, or NP agglomerates, due to interparticle acoustic scattering—the Bjerknes force—grows to dominate. The force can either be repulsive (positive) or attractive (negative) depending on the object size and interobject separation distance.[42] Because in our system we are growing the size of the interacting objects from the starting individual NPs, we consider the 10 μm sized objects already present as the Bjerknes force begins to dominate. These objects are widely spaced as 1D chains across the fluid interface. When the spacing between these objects is *reduced* below about 10 μm from the action of the magnetic field and aided by jostling of the objects by the overall acoustic field, acoustic streaming, and fluid drag, the Bjerknes force becomes attractive and acts to drive the agglomerated objects even closer together, triggering the formation of 2D films of the NPs. These films remain intact long after removal of both the magnetic and acoustic fields, until evaporation grows to dominate.

See supplementary material for details of the Minkowski–Bouligand (MB) dimension calculations of the magnetic nanoparticle structures.

[1] G. M. Whitesides and B. Grzybowski, "Self-assembly at all scales," Science **295**, 2418–2421 (2002).
[2] L. Jiang, X. Chen, N. Lu, and L. Chi, "Spatially confined assembly of nanoparticles," Acc. Chem. Res. **47**, 3009–3017 (2014).
[3] E. Braun, Y. Eichen, U. Sivan, and G. Ben-Yoseph, "DNA-templated assembly and electrode attachment of a conducting silver wire," Nature **391**, 775–778 (1998).
[4] K. Takazawa, Y. Kitahama, Y. Kimura, and G. Kido, "Optical waveguide self-assembled from organic dye molecules in solution," Nano Lett. **5**, 1293–1296 (2005).
[5] X. Li, L. E. Sinks, B. Rybtchinski, and M. R. Wasielewski, "Ultrafast aggregate-to-aggregate energy transfer within self-assembled light-harvesting columns of zinc phthalocyanine tetrakis (perylenediimide)," J. Am. Chem. Soc. **126**, 10810–10811 (2004).
[6] N. Chaki and K. Vijayamohanan, "Self-assembled monolayers as a tunable platform for biosensor applications," Biosens. Bioelectron. **17**, 1–12 (2002).
[7] M. Liong, J. Lu, M. Kovochich, T. Xia, S. G. Ruehm, N. Andre, E. F. Tamanoi, and J. I. Zink, "Multifunctional inorganic nanoparticles for imaging, targeting and drug delivery," ACS Nano **2**, 889 (2008).
[8] A. Edrington, A. Urbas, P. DeRege, C. Chen, T. Swager, N. Hadjichristidis, M. Xenidou, L. Fetters, J. Joannopoulos, and Y. Fink, "Polymer-based photonic crystals," Adv. Mater. **13**, 421–425 (2001).

[9]Y. Sahoo, M. Cheon, S. Wang, H. Luo, E. Furlani, and P. Prasad, "Field-directed self-assembly of magnetic nanoparticles," J. Phys. Chem. B **108**, 3380–3383 (2004).
[10]S. Soeya, J. Hayakawa, H. Takahashi, K. Ito, C. Yamamoto, A. Kida, H. Asano, and M. Matsui, "Development of half-metallic ultrathin fe3o4 films for spin-transport devices," Appl. Phys. Lett. **80**, 823–825 (2002).
[11]D. Coey, A. Berkowitz, L. Balcells, F. Putris, and A. Barry, "Magnetoresistance of chromium dioxide powder compacts," Phys. Rev. Lett. **80**, 3815 (1998).
[12]S. Sun and H. Zeng, "Size-controlled synthesis of magnetite nanoparticles," J. Am. Chem. Soc. **124**, 8204–8205 (2002).
[13]M. Tanase, D. Silevitch, A. Hultgren, L. Bauer, P. Searson, G. Meyer, and D. Reich, "Magnetic trapping and self-assembly of multicomponent nanowires," J. Appl. Phys. **91**, 8549–8551 (2002).
[14]J. Wang, Q. Chen, C. Zeng, and B. Hou, "Magnetic-field-induced growth of single-crystalline fe3o4 nanowires," Adv. Mater. **16**, 137–140 (2004).
[15]M. Wu, Y. Xiong, Y. Jia, H. Niu, H. Qi, J. Ye, and Q. Chen, "Magnetic field-assisted hydrothermal growth of chain-like nanostructure of magnetite," Chem. Phys. Lett. **401**, 374–379 (2005).
[16]D. Choi, S. Jang, H. Yu, and S. Yang, "Two-dimensional polymer nanopattern by using particle-assisted soft lithography," Chem. Mater. **16**, 3410–3413 (2004).
[17]S. Shoji and S. Kawata, "Photofabrication of three-dimensional photonic crystals by multibeam laser interference into a photopolymerizable resin," Appl. Phys. Lett. **76**, 2668–2670 (2000).
[18]S. Xuan, F. Wang, J. M. Y. Lai, K. W. Y. Sham, Y.-X. J. Wang, S.-F. Lee, J. C. Yu, C. H. K. Cheng, and K. C.-F. Leung, "Synthesis of biocompatible, mesoporous fe3o4 nano/microspheres with large surface area for magnetic resonance imaging and therapeutic applications," ACS Appl. Mater. Interfaces **3**, 237–244 (2011).
[19]S. Zhang, M. Regulacio, and M. Han, "Self-assembly of colloidal one-dimensional nanocrystals," Chem. Soc. Rev. **43**, 2301–2323 (2014).
[20]S. Sun, S. Anders, H. F. Hamann, J.-U. Thiele, J. Baglin, T. Thomson, E. E. Fullerton, C. Murray, and B. D. Terris, "Polymer mediated self-assembly of magnetic nanoparticles," J. Am. Chem. Soc. **124**, 2884–2885 (2002).
[21]H. Niu, Q. Chen, H. Zhu, Y. Lin, and X. Zhang, "Magnetic field-induced growth and self-assembly of cobalt nanocrystallites," J. Mater. Chem. **13**, 1803–1805 (2003).
[22]R. White and F. Voltmer, "Direct piezoelectric coupling to surface elastic waves," Appl. Phys. Lett. **7**, 314–316 (1965).
[23]J. Friend and L. Yeo, "Microscale acoustofluidics: Microfluidics driven via acoustics and ultrasonics," Rev. Mod. Phys. **83**, 647 (2011).
[24]S. Levine, B. D. Bowen, and S. J. Partridge, "Stabilization of emulsions by fine particles i. partitioning of particles between continuous phase and oil/water interface," Colloids Surf. **38**, 325–343 (1989).
[25]C. Bradley, "Acoustic streaming field structure: The influence of the radiator," J. Acoust. Soc. Am. **100**, 1399–1408 (1996).
[26]R. Shilton, M. Tan, L. Yeo, and J. R. Friend, "Particle concentration and mixing in microdrops driven by focused surface acoustic waves," J. Appl. Phys. **104**, 014910 (2008).
[27]R. Erb, H. Son, B. Samanta, V. Rotello, and B. Yellen, "Magnetic assembly of colloidal superstructures with multipole symmetry," Nature **457**, 999–1002 (2009).
[28]A. Reenen, A. Jong, and M. Prins, "Transportation, dispersion and ordering of dense colloidal assemblies by magnetic interfacial rotaphoresis," Lab Chip **15**, 2864–2871 (2015).
[29]K. Butter, P. Bomans, P. Frederik, G. Vroege, and A. Philipse, "Direct observation of dipolar chains in iron ferrofluids by cryogenic electron microscopy," Nat. Mater. **2**, 88–91 (2003).
[30]S. Singamaneni, V. N. Bliznyuk, C. Binek, and E. Y. Tsymbal, "Magnetic nanoparticles: Recent advances in synthesis, self-assembly and applications," J. Mater. Chem. **21**, 16819–16845 (2011).
[31]S. Biswal and A. Gast, "Rotational dynamics of semiflexible paramagnetic particle chains," Phys. Rev. E **69**, 041406 (2004).
[32]J. Armstrong, R. Wenby, H. Meiselman, and T. Fisher, "The hydrodynamic radii of macromolecules and their effect on red blood cell aggregation," Biophys. J. **87**, 4259–4270 (2004).
[33]J. Li, Q. Du, and C. Sun, "An improved box-counting method for image fractal dimension estimation," Pattern Recognit. **42**, 2460–2469 (2009).
[34]M. K. Tan, J. R. Friend, and L. Yeo, "Microparticle collection and concentration via a miniature surface acoustic wave device," Lab Chip **7**, 618–625 (2007).
[35]M. Hejazian, W. Li, and N. Nguyen, "Lab on a chip for continuous-flow magnetic cell separation," Lab Chip **15**, 959–970 (2015).
[36]A. Mehdizadeh, R. Mei, J. F. Klausner, and N. Rahmatian, "Interaction forces between soft magnetic particles in uniform and non-uniform magnetic fields," Acta Mech. Sin. **26**, 921–929 (2010).
[37]M. Kim and Z. andrew, "Effect of electrostatic, hydrodynamic and brownian forces on particle trajectories and sieving in normal flow filtration," J. Colloid Interface Sci. **269**, 425–431 (2004).
[38]K. Berland, V. Cooper, K. Lee, E. Schröder, T. Thonhauser, P. Hyldgaard, and B. Lundqvist, "van der Waals forces in density functional theory: A review of the vdW-DF method," Rep. Prog. Phys. **78**, 066501 (2015).
[39]P. Kralchevsky and K. Nagayama, "Capillary forces between colloidal particles," Langmuir **10**, 23–36 (1994).
[40]F. Nadal and E. Lauga, "Small acoustically forced symmetric bodies in viscous fluids," J. Acoust. Soc. Am. **139**, 1081–1092 (2016).
[41]M. Miansari, A. Qi, L. Yeo, and J. R. Friend, "Vibration-induced deagglomeration and shear-induced alignment of carbon nanotubes in air," Adv. Funct. Mater. **25**, 1014–1023 (2015).
[42]T. Laurell, F. Petersson, and N. andreas, "Chip integrated strategies for acoustic separation and manipulation of cells and particles," Chem. Soc. Rev. **36**, 492–506 (2007).
[43]J. N. Israelachvili, *Intermolecular and Surface Forces: Revised Third Edition* (Academic Press, 2011).
[44]B. Faure, G. Salazar-Alvarez, and L. Bergström, "Hamaker constants of iron oxide nanoparticles," Langmuir **27**, 8659–8664 (2011).
[45]H. C. Hamaker, "The London—van der Waals attraction between spherical particles," Physica **4**, 1058–1072 (1937).
[46]H. Shinto, D. Komiyama, and K. Higashitani, "Lateral capillary forces between solid bodies on liquid surface: A lattice Boltzmann study," Langmuir **22**, 2058–2064 (2006).
[47]P. A. Kralchevsky and N. D. Denkov, "Capillary forces and structuring in layers of colloid particles," Curr. Opin. Colloid Interface Sci. **6**, 383–401 (2001).
[48]C. Balanis, *Advanced Engineering Electromagnetics* (John Wiley & Sons, 2012).
[49]D. Reeves and J. Weaver, "Simulations of magnetic nanoparticle Brownian motion," J. Appl. Phys. **112**, 124311 (2012).
[50]Y. Min, M. Akbulut, K. Kristiansen, Y. Golan, and J. Israelachvili, "The role of interparticle and external forces in nanoparticle assembly," Nat. Mater. **7**, 527–538 (2008).